Electronic Subband Reconfiguration in a d^0-Perovskite Induced by Strain-Driven Structural Transformations

V. Laukhin,[1,2] O. Copie,[3,*] M. J. Rozenberg,[4] R. Weht,[5,6] K. Bouzehouane,[3] N. Reyren,[3] E. Jacquet,[3] M. Bibes,[3] A. Barthélémy,[3] and G. Herranz[1,†]

[1]*Institut de Ciència de Materials de Barcelona (ICMAB-CSIC), Campus de la UAB, Bellaterra 08193, Catalonia, Spain*
[2]*Institució Catalana de Recerca i Estudis Avançats (ICREA), 08010 Barcelona, Catalonia, Spain*
[3]*Unité Mixte de Physique CNRS/Thales, 1 avenue Fresnel, Campus de l'Ecole Polytechnique, 91767 Palaiseau, France and Université Paris-Sud, 91405 Orsay, France*
[4]*Laboratoire de Physique des Solides, Université Paris-Sud, Bâtiment 510, 91405 Orsay, France*
[5]*Gerencia de Investigación y Aplicaciones, Comisión Nacional de Energía Atómica (CNEA), Avenida General Paz y Constituyentes, 1650-San Martín, Argentina*
[6]*Instituto Sabato, Universidad Nacional de San Martín-CNEA, 1650-San Martín, Argentina*

(Received 20 February 2012; revised manuscript received 19 June 2012; published 28 November 2012)

It is well known that transport in lightly *n*-doped $SrTiO_3$ involves light and heavy electron bands. We have found that upon application of moderate quasi-isotropic pressures, the relative positions of these subbands are changed by a few meV and, eventually, a band inversion occurs at ~1 kbar. Such effects are, however, suppressed in the closely related $KTaO_3$ perovskite. We show that the extremely subtle electronic reconfiguration in $SrTiO_3$ is triggered by strain-induced structural transformations that are accompanied by remarkable mobility enhancements up to about $\Delta\mu/\mu \approx 300\%$. Our results provide a microscopic rationale for the recently discovered transport enhancement under strain and underscore the role of the internal structural degrees of freedom in the modulation of the perovskite electronic properties.

DOI: 10.1103/PhysRevLett.109.226601 PACS numbers: 72.10.−d, 71.20.−b, 73.20.−r

The recent discovery of high-mobility transport in oxide heterostructures [1] has attracted the investigation of these systems for novel applications, with $SrTiO_3$ as the powerhouse of this emerging electronics [2]. Strontium titanate is a band insulator that goes into a conductive state by chemical or electrostatic doping [3,4]. Extremely confined highly conductive layers can be created when interfacing $SrTiO_3$ with polar oxides (e.g., $LaAlO_3$) [1] or at the bare surface of $SrTiO_3$ crystals [5,6]. Underlying all these transport properties is the fact that the electronic mobility of the $SrTiO_3$ structures can reach values above 10^4 $cm^2/V\,s$, among the highest in any bulk oxide [1,3]. Spectacular advances in high-quality complex $SrTiO_3$ heterostructures have demonstrated the feasibility of boosting those remarkable transport properties even more and, in particular, of enhancing the electron mobility of $SrTiO_3$ [7,8]. An interesting complementary pathway is provided by the modulation of internal structural degrees of freedom [9]. This idea has been already successfully applied to other materials, and a remarkable example is given by recent developments of electron band modification in silicon-based devices through strain engineering [10], leading to mobility enhancement factors above 100% in Si/SiGe structures [10,11].

Similar to conventional semiconductors, it has been recently found that strain induces also a large enhancement of the mobility in $SrTiO_3$, which opens up promising avenues to tailor the properties of high-mobility $SrTiO_3$ structures [8,12]. Nevertheless, the microscopic understanding of the strain-dependent electronic band structure—crucial to understand this extraordinary transport enhancement—is not well understood. Interestingly, pressure is expected to be a significant driving force to induce important changes in the electronic structure because the Fermi energy of lightly doped $SrTiO_3$ is just a few meV from the bottom of the conduction band [13]. In consequence, here we have considered the systematic variations of transport under quasi-hydrostatic pressure as an extremely sensitive probe of the conduction states. We have discovered a nonmonotonic strain dependence of mobility and carrier density that can only be interpreted in a multiband framework in which light and heavy electrons participate in transport. We have found that the subband energy splittings are about a few meV at ambient pressure, but a moderate pressure—in the order of ~1 kbar—is sufficient to modulate the subband structure and even trigger a band inversion that is accompanied by mobility increases of around 300%. Such a strain-modulated electronic structure is suppressed in $KTaO_3$, a perovskite with closely related electronic properties [14] that can also sustain two-dimensional surface metallic states [15,16]. We show that the mobility enhancement in $SrTiO_3$ is set off by a very subtle rearrangement of electrons among the conduction subband states driven by strain-induced structural transformations that are, however, absent in $KTaO_3$.

We analyzed two $SrTiO_3$ (samples *A* and *B*) and one $KTaO_3$ single crystals that were doped with a different amount of carriers via thin film deposition (see sample

preparation conditions in the Supplemental Material [17]). The electronic homogeneity was carefully checked by transport (Fig. S1 in the Supplemental Material [17]). For pressure experiments, we placed the samples in a clamp-type piston cylinder pressure cell that used an organic liquid as a pressure transmitting medium [18]. The decrease of pressure when cooling was properly corrected and the temperature was varied at low rates to approach the quasihydrostatic pressure condition.

From Hall transport measurements we extracted the mobility μ and sheet carrier density n_{sheet} for various pressures ($P \sim 10^{-3}$–10 kbar) and temperatures ($T \sim$ 5 K–150 K). Assuming a uniform carrier distribution, the effective carrier density $n(P)$—which, in general, is a function of the pressure P—was inferred after dividing n_{sheet} by the crystal thickness. In particular, at ambient pressure, we obtained for $SrTiO_3$ volume carrier concentrations $n_0 \approx 1.1 \times 10^{18}$ cm^{-3} (sample A) and $n_0 \approx 8 \times 10^{18}$ cm^{-3} (sample B), with low temperature (5 K) mobilities $\mu \approx 3 \times 10^3$ cm^2/V s (sample A) and $\mu \approx 0.35 \times 10^3$ cm^2/V s (sample B). The μ vs n data shown in Fig. S2 (Supplemental Material [17]) show that these two samples are representative of the properties of metallic $SrTiO_3$ in the μ-n diagram [13]. For $KTaO_3$ we found $n_0 \approx 5.25 \times 10^{15}$ cm^{-3} and $\mu \approx 0.785 \times 10^3$ cm^2/V s.

The dependence of n_{sheet} and μ on pressure measured at various temperatures is displayed in Fig. 1. Note first the striking dissimilar pressure dependence between $SrTiO_3$ and $KTaO_3$. While the n_{sheet} for $KTaO_3$ is decreasing rather monotonically for pressure values above 1 kbar, for $SrTiO_3$ a conspicuous dip in the sheet carrier density is observed at the lowest temperatures ($T \leq 10$ K for sample A and $T \leq 35$ K for sample B), indicating an *apparent* sharp carrier depletion at pressures $P \sim 1$ kbar, which could be initially interpreted as a significant carrier freezing. On the other hand, the mobility of $KTaO_3$ shows modest variations for all the range of applied pressures, with a maximum decrease at the lowest temperature of $\approx -20\%$ from ambient to the highest pressure. In contrast, the mobility of $SrTiO_3$ exhibits a cusplike pressure dependence, with its peak value at around the pressure of the apparent sheet carrier density dip. The mobility enhancement is strongest at lower temperatures, being about $\Delta\mu/\mu \approx 300\%$ for sample A, and $\Delta\mu/\mu \approx 115\%$ for sample B at temperature $T = 5$ K.

While the physical origin of the strikingly different behavior of $SrTiO_3$ and $KTaO_3$ is discussed at the end, henceforth we will focus our analysis to $SrTiO_3$. Note that the interpretation of the observed nonmonotonic behavior in a single-band picture would require unrealistic large modulations of the carrier effective masses (see discussion in the Supplemental Material [17]). Instead, we show that the data can be satisfactorily described within a two-band model with heavy and light electrons with an effective carrier density given by [19]:

$$n(P) = \frac{(\mu_l n_l)^2 + (\mu_h n_h)^2}{\mu_l^2 n_l + \mu_h^2 n_h} \tag{1}$$

where μ_l, μ_h, n_l, n_h are the mobility and volume carrier densities of light and heavy electrons, respectively, which are all dependent on pressure. Note that in Eq. (1) the terms dependent on the magnetic field are neglected [19], since the Hall coefficients stay constant for all magnetic fields up to $B = 9$ T, except for singular cases that are discussed at the end (see also Fig. 4). The electrons are unequally populating the light and heavy bands, giving way to a population unbalance $\Delta n_{lh} = n_l - n_h$ determined by the energy splitting $\Delta_{lh}(P)$ between both bands. We assume in the following that the total number of carriers stays constant for all pressures; i.e., the sum of the carrier densities of light and heavy electrons is equal to $n_0 = n_l + n_h$.

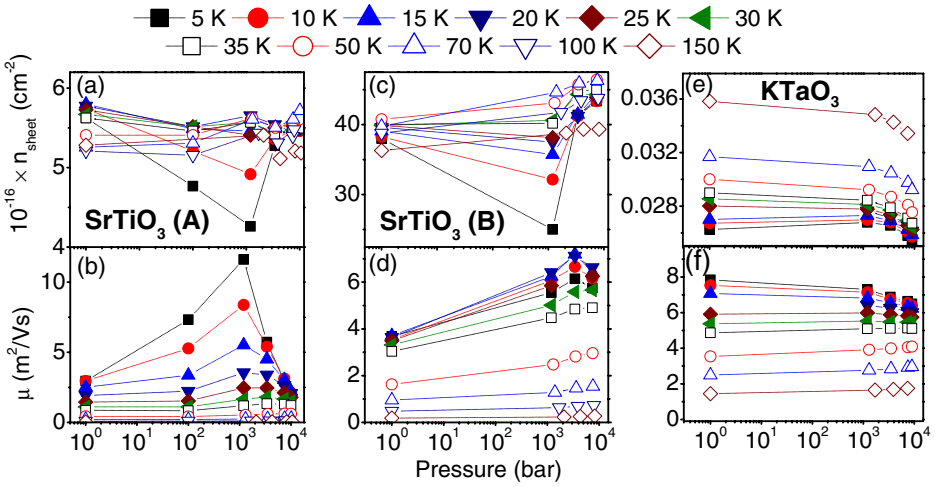

FIG. 1 (color online). Sheet carrier density n_{sheet} and the electron mobility μ as a function of pressure (corrected for temperature) measured at different temperatures, for $SrTiO_3$ samples A (a), (b) and B (c), (d) and for $KTaO_3$ (e), (f).

The two-band model has the obvious advantage of not requiring unrealistic assumptions about huge strain-driven effective mass enhancements and it offers a natural way to understand the sheet carrier density dip (Fig. 1). Indeed, conduction band splittings have been inferred experimentally [5,20–25] and supported by theory [26–28]. To better set the discussion, we define the mobility ratio $b = \mu_l/\mu_h$, the relative volume-carrier density $n^r = n/n_0$ and the relative differential band populations $\Delta n^r_{lh} = \Delta n_{lh}/n_0$, so that we can parametrize Eq. (1) as:

$$n^r = \frac{[(1+b) + \Delta n^r_{lh}(b-1)]^2}{2[b^2 + 1 + \Delta n^r_{lh}(b^2-1)]}. \quad (2)$$

Figure 2 shows the predicted behavior of n^r as a function of Δn^r_{lh}, obtained from Eq. (2), for three different values of the parameter b. Remarkably, the dip in the experimental sheet carrier density (Fig. 1) is reproduced by $n^r(\Delta n^r_{lh})$ (Fig. 2) without the need of invoking any *real* carrier freezing. Thus, Eq. (2)—parametrized in terms of the mobility ratio (b), relative volume-carrier density (n^r), and differential band population (Δn^r_{lh})—can appropriately describe the observed pressure dependence of transport, and will be considered in the following to understand the evolution with strain of the energy splitting $\Delta_{lh}(P)$.

The values of Δn^r_{lh} extracted from experiments are plotted in Fig. 2 for sample A (stars) and sample B (squares). The values $\Delta n^r_{lh} < 0$ (area not shaded in Fig. 2) correspond to the case when the heavy band is populated preferentially, while $\Delta n^r_{lh} > 0$ (shaded area) indicates that the electrons occupy mainly the light band. Because Eq. (2) is quadratic, two sets of solutions for Δn^r_{lh} are found. At pressures close to the ambient the two solutions correspond to $\Delta n^r_{lh} < 0$ (full symbols) and $\Delta n^r_{lh} > 0$ (hollow symbols), respectively. At high enough pressures, $P \sim 1$ kbar, the sign of Δn^r_{lh} is reversed for both sets, so that a band inversion occurs for both cases. Because the mobility is enhanced by increasing the pressure just above the ambient, carriers should populate mostly the heavy band at ambient pressure, and the light band is progressively occupied with pressure, thus increasing the mobility (full symbols in Fig. 2). We note that while theoretical [26] and experimental works [5,25] report lowest energy light bands in surfaces and interfaces, first-principles calculations indicate that the lowest band has larger mass in bulk [27,29].

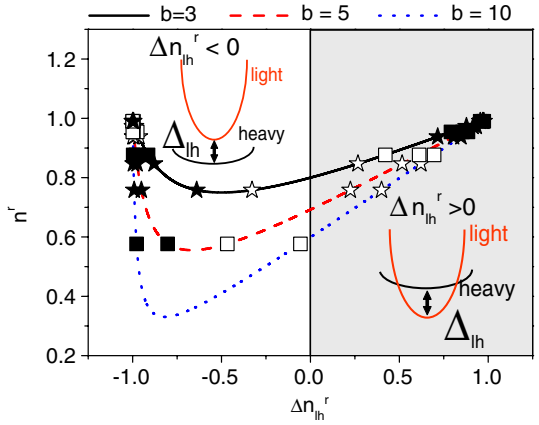

FIG. 2 (color online). Calculated curves of the relative carrier density n^r versus the relative differential band population Δn^r_{lh} for different values of the mobility ratio parameter b [Eq. (2)]. The experimental values of n^r are plotted as stars (sample A) and squares (sample B). The shaded (not shaded) areas correspond to $\Delta n^r_{lh} > 0$ ($\Delta n^r_{lh} < 0$).

To determine the energy splitting Δ_{lh} between light and heavy bands as a function of pressure we have used the Chang-Izabelle approximation, which gives a maximum error of $\sim$1% for the considered full range of energies with respect to the exact calculation based on the Fermi-Dirac integral [30]. For the calculation of the carrier density in this approximation we have

$$\Delta_{l(h)} = k_B T\left\{\ln\frac{n_0 \pm \Delta n_{l(h)}}{N_{l(h)}(n_0 \pm \Delta n_{l(h)})} + \left[\frac{3}{2}\Gamma(3/2)\right]^{2/3} \times \frac{[n_0 \pm \Delta n_{l(h)}]/[2N_{l(h)}]}{[0.59 + (n_0 \pm \Delta n_{l(h)})/(2N_{l(h)})]^{1/3}}\right\}, \quad (3)$$

where $\Delta_{l(h)}$ represents the position of the Fermi energy with respect to the bottom of the light (heavy) conduction band, $+(-)$ applies to light (heavy) electrons, and $N_{l(h)}$ is the effective density of states of light (heavy) bands defined as $N_{l(h)} = \frac{1}{4}[\frac{2m^*_{l(h)}k_BT}{\hbar^2\pi}]^{3/2}$, where $m^*_{l(h)}$ is the effective mass of light (heavy) electrons, respectively. We have taken the approximation that the mobility ratio is roughly the inverse ratio of the effective masses, i.e., $b = \mu_l/\mu_h = m^*_h/m^*_l$. Recent band structure calculations and experimental findings indicate that the mass ratio is $m^*_h/m^*_l \approx 10$–20 [5,31], so that we assume a similar valor for the parameter b. A roughly similar mobility ratio has been inferred from magnetotransport experiments [20]. From the derived $\Delta n^r_{lh}(P)$ dependence and assuming that $b = 10$ and $m^*_l \approx m^*_0$ (bare electron mass), we have obtained the energy splitting $\Delta_{lh} = \Delta_l - \Delta_h$ between light and heavy bands as a function of the applied pressure at $T = 5$ K (see Fig. 3). We have checked that the energy splittings Δ_{lh} are not strongly modified by considering different mobility ratios (Fig. 3) or effective masses (Fig. S3 in the Supplemental Material [17]). An inspection of Fig. 3 allows us to conclude that (i) the light and heavy bands cross each other at some intermediate pressure, close to $P \sim 1$ kbar, and (ii) the energy splittings Δ_{lh} are of the order of the meV. This offers a natural way to explain why the dip in $n_{\text{sheet}}(P)$ (Fig. 1) is observed only at low temperature where $k_BT \lesssim \Delta_{lh}$. For temperatures above around 10–15 K the influence

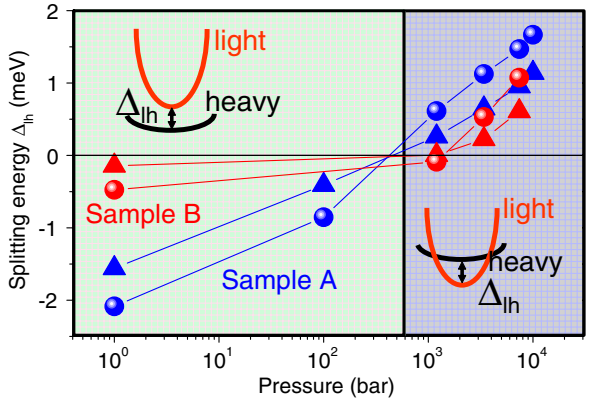

FIG. 3 (color online). Pressure dependence of Δ_{lh} at $T = 5$ K as calculated from the experiments through Eq. (3) for both samples A (blue) and B (red). Mobility ratios $b = 5$ (triangles) and $b = 10$ (circles) have been used to calculate these values.

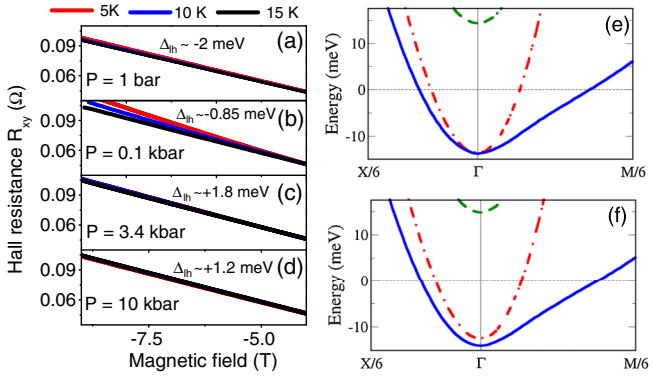

FIG. 4 (color online). Hall resistance R_{xy} of sample A measured at (a) $P \approx 10^{-3}$ kbar, (b) $P \approx 0.1$ kbar, (c) $P \approx 3.4$ kbar and (d) $P \approx 10$ kbar. The values of the splitting Δ_{lh} indicated in the panels are those extracted from Fig. 3 assuming $b = 10$. Bands calculated from density functional theory are shown in (e) and (f) for the cubic and tetragonal structure, respectively. The spin orbit splits the bands into an upper singlet (dashed green) and doublet with light (dashed-dotted red) and heavy (solid blue) masses.

of the energy splitting is rapidly smeared out by thermal effects, in perfect agreement with experiments.

As a further check of the consistency of our analysis, we have analyzed the evolution of the Hall resistance R_{xy} as a function of pressure and temperature. For fields $|B| \leq 9$ T the maximum cyclotron energy is $\hbar\omega_c = \frac{\hbar eB}{m^*_{l(h)}} \approx 1$ meV. Since the sheet carrier density is obtained from the Hall resistance through $n_{\text{sheet}} = B/(eR_{xy})$, a nonlinear $R_{xy}(B)$ is only expected at low enough temperatures ($T \lesssim 15$ K) and small band splittings ($\Delta_{lh} \lesssim 1$ meV). This is just what we observe in Figs. 4(a)–4(d), where $R_{xy}(B)$ displays an almost perfect linear dependence on magnetic field (up to $B = 9$ T) except when measured at $T \leq 10$ K and pressure $P \approx 0.1$ kbar, where the splitting energy is estimated to be $\Delta_{lh} \approx -0.5$–0.8 meV for sample A.

To shed light on the microscopic mechanisms, we have carried out density functional theory calculations (see details in the Supplemental Material [17]). According to them, in the cubic structure, the spin-orbit coupling (Δ_{SO}) splits the degenerate t_{2g} bands by ~30 meV at the Γ point, giving way to a low-lying doublet with a heavy and a light band, plus a higher energy singlet state with a light mass [Fig. 4(e)]. Note that, because of the very small Fermi energy (~ meV), only the low-lying doublet states are relevant for transport. Additionally, below $T \lesssim 105$ K, $SrTiO_3$ undergoes an antiferrodistortive cubic-to-tetragonal transformation involving rigid TiO_6 octahedra rotations in opposite directions around the c axis [27] that results in a tetragonal unit cell with a lattice parameter ratio $c/a \approx 1.0008$. This causes a splitting of the degenerate low-lying doublet leading, at ambient pressure, to two strongly mixed bands separated by a few meV [see Fig. 4(f)], in perfect agreement with the experiments. We have also investigated the effects on the electronic structure of varying the cell tetragonality c/a ratio, which is known to be enhanced with hydrostatic pressure [32]. From this study we conclude that if c/a decreases and eventually goes below unity, the splitting energy between the upper light and the lower heavy bands is reduced, and eventually they reverse their positions, as observed in the experiments [33]. Such a scenario should imply strain-driven structural transformations with symmetry lower than tetragonal [34], in which both octahedra rotations and tiltings should occur. Further experimental work is needed to validate these predictions.

Finally, we observe that $KTaO_3$ remains cubic down to the lowest temperatures [27] with no indications of pressure-induced transition to tetragonality [35]. This explains why, contrary to $SrTiO_3$, a band inversion and a nonmonotonic strain dependence of n_{sheet} and μ are absent in $KTaO_3$. From the $SrTiO_3$ mechanical properties [36] we can infer a lattice deformation $\simeq 0.02\%$ at the band crossing point ($P \approx 1$ kbar). Epitaxial strain engineering is then suggested to be an invaluable strategy towards transport enhancement in $SrTiO_3$. Although we have used quasi-isotropic instead of uniaxial or biaxial strain, it is known that both hydrostatic and nonhydrostatic stress yield similar distortions and tiltings of TiO_6 octahedra in a closely related perovskite, $CaTiO_3$ [37]. Therefore, we believe that our results give a suitable description of the physical mechanisms that govern the recently observed large mobility enhancements with uniaxial strains [12] and illustrate the enticing opportunities that an accurate control of octahedral rotations offer to engineer the material properties in perovskites [9,38].

This work was supported by the Spanish MAT2011-29269-C03 and NANOSELECT CSD2007-00041 projects, the Generalitat de Catalunya (2009 SGR 00376 project) and the French ANR OXITRONICS. We warmly acknowledge discussions on the subject with A. F. Santander-Syro.

*Present address: CRISMAT, CNRS-ENSICAEN UMR6508, 6 Boulevard du Maréchal Juin, F-14050 Caen Cedex 4, France.
†gherranz@icmab.es

[1] A. Ohtomo and H. Y. Hwang, Nature (London) **427**, 423 (2004).
[2] J. Mannhart and D. Schlom, Science **327**, 1607 (2010).
[3] O. N. Tufte and P. W. Chapman, Phys. Rev. **155**, 796 (1967).
[4] K. Ueno, S. Nakamura, H. Shimotani, A. Ohtomo, N. Kimura, T. Nojima, H. Aoki, Y. Iwasa, and M. Kawasaki, Nature Mater. **7**, 855 (2008).
[5] A. F. Santander-Syro *et al.*, Nature (London) **469**, 189 (2011).
[6] W. Meevasana, P. D. C. King, R. H. He, S.-K. Mo, M. Hashimoto, A. Tamai, P. Songsiriritthigul, F. Baumberger, and Z.-X. Shen, Nature Mater. **10**, 114 (2011).
[7] Y. Kozuka, M. Kim, C. Bell, B. G. Kim, Y. Hikita, and H. Y. Hwang, Nature (London) **462**, 487 (2009).
[8] J. Son, P. Moetakef, B. Jalan, O. Bierwagen, N. J. Wright, R. Engel-Herbert, and S. Stemmer, Nature Mater. **9**, 482 (2010).
[9] J. M. Rondinelli and N. A. Spaldin, Phys. Rev. B **82**, 113402 (2010).
[10] Y. Song, H. Zhou, Q. Xu, J. Luo, H. Yin, J. Yan, and H. Zhong, J. Electron. Mater. **40**, 1584 (2011).
[11] L. Smith, V. Moroz, G. Eneman, P. Verheyen, F. Nouri, L. Washington, M. Jurczak, O. Penzin, D. Pramanik, and K. De Meyer, IEEE Electron Device Lett. **26**, 652 (2005).
[12] B. Jalan, S. J. Allen, G. E. Beltz, P. Moetakef, and S. Stemmer, Appl. Phys. Lett. **98**, 132 102 (2011).
[13] G. Herranz *et al.*, Phys. Rev. Lett. **98**, 216803 (2007).
[14] L. F. Mattheiss, Phys. Rev. B **6**, 4718 (1972).
[15] P. King *et al.*, Phys. Rev. Lett. **108**, 117602 (2012).
[16] A. F. Santander-Syro *et al.*, Phys. Rev. B **86**, 121107(R) (2012).
[17] See Supplemental Material at http://link.aps.org/supplemental/10.1103/PhysRevLett.109.226601 for details on transport characterization and analysis and on density functional theory calculations.
[18] V. Laukhin, B. Martínez, J. Fontcuberta, and Y. M. Mukovskii, Phys. Rev. B **63**, 214417 (2001).
[19] J. Ziman, *Principles of the Theory of Solids* (Cambridge University Press, Cambridge, England, 1972), 2nd ed.
[20] M. Ben Shalom, A. Ron, A. Palevski, and Y. Dagan, Phys. Rev. Lett. **105**, 206401 (2010).
[21] H. Uwe, R. Yoshizaki, T. Sakudo, A. Izumi, and T. Uzumaki, Jpn. J. Appl. Phys. **24**, 335 (1985).
[22] B. Gregory, J. Arthur, and G. Seidel, Phys. Rev. B **19**, 1039 (1979).
[23] M. Salluzzo *et al.*, Phys. Rev. Lett. **102**, 166804 (2009).
[24] K.-J. Zhou, M. Radovic, J. Schlappa, V. Strocov, R. Frison, J. Mesot, L. Patthey, and T. Schmitt, Phys. Rev. B **83**, 201402(R) (2011).
[25] Y. J. Chang, A. Bostwick, Y. S. Kim, K. Horn, and E. Rotenberg, Phys. Rev. B **81**, 235109 (2010).
[26] P. Delugas, A. Filippetti, V. Fiorentini, D. I. Bilc, D. Fontaine, and P. Ghosez, Phys. Rev. Lett. **106**, 166807 (2011).
[27] L. F. Mattheiss, Phys. Rev. B **6**, 4740 (1972).
[28] Z. S. Popovic, S. Satpathy, and R. M. Martin, Phys. Rev. Lett. **101**, 256801 (2008).
[29] A. Janotti, D. Steiauf, and C. G. Van de Walle, Phys. Rev. B **84**, 201304(R) (2011).
[30] T. Y. Chang and A. Izabelle, J. Appl. Phys. **65**, 2162 (1989).
[31] D. van der Marel, J. L. M. van Mechelen, and I. I. Mazin, Phys. Rev. B **84**, 205111 (2011).
[32] M. Guennou, P. Bouvier, J. Kreisel, and D. Machon, Phys. Rev. B **81**, 054115 (2010).
[33] Across the band crossing the effective masses of light and heavy electronic states are renormalized by less that $\approx 25\%$.
[34] A. Grzechnik, G. H. Wolf, and P. F. McMillan, J. Raman Spectrosc. **28**, 885 (1997).
[35] Y. Yacobi, F. Cerdeira, M. Schmidt, and W. B. Holzapfel, Solid State Commun. **14**, 1325 (1974).
[36] A. G. Beattie and G. A. Samara, J. Appl. Phys. **42**, 2376 (1971).
[37] J. Zhao, N. L. Ross, D. Wang, and R. J. Angel, J. Phys. Condens. Matter **23**, 455401 (2011).
[38] J. Rondinelli, S. May, and J. Freeland, MRS Bull. **37**, 261 (2012).